Study on the Applicability of Deterioration Detection Techniques for Sandstone Heritage in Multi Environment using MLP-Attention Model

Chengjin Yan[1,2], Yuan Cheng [1,3], Yue Zhang [1,3], Haomin Yu[4], Jizhong Huang[1,3], Hongbin Yan[5]

[1] Key Laboratory of Silicate Cultural Relics Conservation (Shanghai University), Ministry of Education – yanchengjin2003@shu.edu.cn, chengyuan@shu.edu.cn, 2019zhangy@shu.edu.cn, hjizhong@shu.edu.cn
[2] School of Computer Engineering and Science, Shanghai University, 99 Shangda Road, Shanghai 200444, China – yanchengjin2003@shu.edu.cn
[3] Institute for the Conservation of Cultural Heritage, School of Cultural Heritage and Information Management, Shanghai University, Shanghai, China-chengyuan@shu.edu.cn, 2019zhangy@shu.edu.cn, hjizhong@shu.edu.cn
[4] Department of Computer Science, Aalborg University, Aalborg, Denmark – haominyu@cs.aau.dk
[5] Yungang Research Institute, Datong, China- 435135458@qq.com

Keywords: Stone Cultural Heritage, Degradation Detection, Deep Learning, SEM images.

Abstract

Stone cultural heritage, encompassing a broad spectrum of artifacts such as stone artworks, buildings, tools, and utensils, represents one of the most significant categories of cultural heritage. However, the conservation of these cultural heritage faces challenges from the process of deterioration. This degradation not only compromises the structural integrity of the heritage but also results in the loss of invaluable historical information. Thus, there emerges a critical demand for effective methods to detect and assess the condition of stone cultural heritage, enabling timely and precise conservation interventions. Here we obtained sandstone samples under different deteriorative environments through laboratory-simulated deterioration experiments and employed a variety of detection technologies to capture a series of changes in the deterioration detection parameters during the sandstone deterioration process. Subsequently, a deep learning model was established to correlate the detection parameters with the degree of stone deterioration. A SHAP analysis was then conducted to determine the contribution of various parameters to the degree of stone weathering under different experimental environments, providing recommendations for selecting appropriate detection technologies and indicators adapted to different deterioration environments. To further analyze the deterioration processes of the stone samples, XRD analysis was conducted to observe changes in mineral composition throughout the deterioration process. SEM images were utilized to examine the changes in micro-morphology and the internal pore structure associated with deterioration. This study provides a basis for the scientific design of deterioration detection schemes by selecting the most suitable testing technology for optimal deterioration assessment under specific environmental conditions.

1. Introduction

Stone cultural heritage, encompassing a broad spectrum of artifacts such as stone artworks, buildings, tools, and utensils, represents one of the most significant categories of cultural heritage (Huang et al., 2022). These cultural heritages, characterized by their diverse types, vast quantities, and extensive historical span, are indispensable for understanding the cultural identity and historical continuity of human civilizations. However, the conservation of these cultural heritages faces challenges from the process of deterioration (Zhang et al., 2022). Environmental factors, ranging from temperature and humidity fluctuations to pollution and biological colonization, have significantly contributed to the accelerated degradation of stone cultural heritage. This degradation not only compromises the structural integrity of the heritage but also results in the loss of invaluable historical information. Therefore, there is a critical need for effective methods to detect and assess the condition of stone cultural heritage, enabling timely and precise conservation interventions.

Currently, the assessment of the deterioration degree of stone cultural heritage primarily utilizes three categories of indicators. The first category evaluates deterioration through the physical and mechanical properties of stone, exemplified by the classification of carbonate rocks' weathering degrees based on ultrasonic wave velocity (El-Gohary, 2013; Fioretti and Andriani, 2018), and based on the penetration ratio of weathered rock to fresh rock (Hachinohe et al., 2000). The second category assesses the mineralogical and chemical compositions of stone, such as comparing mineral components before and after deterioration using X-ray diffraction (XRD) analysis (Friolo et al., 2003), and detecting changes in chemical elements with X-ray fluorescence (XRF). The third category focuses on the microscopic features of stone, like micro-fractures and porosity (Ceryan et al., 2008), measuring changes in Al_2O_3, SiO_2, and TiO_2 during the weathering process (Jayawardena and Izawa, 1994), or utilizing the linear fracture density index for evaluation (Sousa et al., 2005). Existing research suggests that the applicability of various deterioration detection techniques in porous stone cultural heritage, such as sandstones, can vary greatly depending on the primary environmental conditions and mechanisms of deterioration. In environments characterized by physical weathering, such as temperature fluctuations, wetting-drying cycles, and freeze-thaw actions, the porosity of sandstone may increase, and internal micro-fractures may form, thereby rendering ultrasonic testing more feasible. Conversely, in environments characterized by chemical weathering, like those affected by atmospheric pollution and acid rain, changes in the mineral composition and chemical elements of sandstone suggest that XRF and XRD detections could be more effective (Yang et al., 2023; Zhang et al., 2023). However, there remains a lack of

systematic guidance for selecting the most suitable testing technology, particularly non-destructive ones, for optimal deterioration assessment under specific environmental conditions (Wang et al., 2024). This hinders the efficient and accurate application of these techniques in practical monitoring and evaluation scenarios.

It is important to study the cross-environmental adaptability of various non-destructive testing methods, thereby providing a basis for the scientific design of deterioration detection schemes. Therefore, this study emphasize the importance of selecting the most appropriate and effective detection parameters and technologies for evaluating stone deterioration, tailored to the specific environmental challenges faced by the stone cultural heritage. We obtained sandstone samples under different deteriorative environments through laboratory-simulated deterioration experiments and employed a variety of detection technologies to capture a series of changes in the deterioration detection parameters during the sandstone deterioration process. Subsequently, a deep learning model was established to correlate the detection parameters with the degree of stone deterioration. A SHAP analysis was then conducted to determine the contribution of various parameters to the degree of stone weathering under different experimental environments, providing recommendations for selecting appropriate detection technologies and indicators adapted to different deterioration environments. Specifically, laboratory-simulated deterioration experiments, involving freeze-thaw cycles, and dry-wet cycles with acidic and alkaline solutions, were conducted to obtain sandstone samples under different weathering environments. In addition to the non-destructive testing methods, this study also implemented destructive testing techniques (including SEM, XRD) to further analyze the deterioration processes of the stone samples. The results indicate that the suitability of various detection technologies for assessing deterioration varies significantly across different environmental conditions, such as acidic, alkaline, and freeze-thaw scenarios. Additionally, the relevance of these detection parameters is closely associated with changes in the microstructure and chemical composition of the stone during the deterioration process. These findings emphasize the importance of selecting the most appropriate and effective detection parameters and technologies for evaluating stone deterioration, tailored to the specific environmental challenges faced by the stone cultural heritage.

The rest of this paper is organized as follows: Section 2 introduces the study area of the experiment and the source of the experimental samples. Section 3 discusses the data format and problem formulation. Section 4 describes the techniques used in the simulation experiments and the organization of the experimental data. Section 5 presents the deep neural network model and the techniques employed during the training process. Section 6 discusses the major findings of the conducted experiments. Finally, the conclusion is presented in Section 7.

2. Study Area and Sandstone Samples

The Yungang Grottoes are a UNESCO World Heritage site, with the earliest carvings dating back to the time of the Xiaowen Emperor of the Northern Wei Dynasty (398-403 AD). Located at 113°20' E, 40°04' N, in the southern foothills of the Wuzhou Mountains in Datong City, Shanxi Province, China, the grottoes extend for about 1 km along the mountainside from east to west, covering an area of over 20,000 square meters. Currently, there are 45 major caves, 252 niches of varying sizes, and a total of more than 51,000 stone sculptures.

The Yungang area experiences a continental semi-arid monsoon climate, with significant diurnal and seasonal temperature variations. Summers are extremely hot and rainy, while winters are dry and cold. The diurnal temperature difference can reach up to 20°C, and the monthly temperature difference can be as high as 40°C, with an average temperature of around 23°C in July. The average annual freezing period lasts 150 days. The annual average precipitation is 430 mm, but in extreme cases, it can exceed 600 mm or be as low as 140 mm, mainly concentrated in July and August, with relative humidity reaching 80%, which can lead to short-term high-temperature heavy rainfall events. Under these climatic conditions, the sandstone of the Yungang Grottoes undergoes frequent freeze-thaw cycles due to the internal moisture phase changes. This long-term freeze-thaw process continuously weakens the structural integrity of the sandstone, increasing porosity, expanding cracks, and ultimately causing irreversible structural damage. It is evident that physical weathering is a significant cause of the deterioration of the Yungang Grottoes sandstone relics, posing a serious threat to their preservation.

The air around the Yungang Grottoes contains suspended particles, carbon dioxide, sulfur dioxide, and other nitrogen oxides. These gaseous pollutants, combined with factors such as moisture and temperature, undergo multi-factor coupling, directly causing chemical erosion and damage to the sandstone in the grottoes. Additionally, due to the continuous dissolution of deep-seated minerals, groundwater is often not neutral but exists in acidic or alkaline forms. Under the action of water and acid-base chemical corrosion, the mechanical strength of the sandstone decreases, and its cementing ability also decreases, leading to problems such as particle loss and cracks in the sandstone, posing a significant threat to the preservation of the grotto sculptures.

This study selected sandstone from the Yungang Grottoes as the experimental object and conducted simulated weathering experiments in the laboratory. To ensure that the structural properties of the experimental samples are as consistent as possible with the actual grottoes, we collected sandstone samples near the Yungang Grottoes scenic area to prevent any impact on the grottoes. The collected samples were fresh rocks excavated during recent construction, with uniform texture, clear grain, and a yellowish brown color, which fully meeting the requirements for fresh sandstone experiments.

3. Experiments and Detection Techniques

3.1 Simulated Weathering Experiments

After sampling and preparation, the sandstone samples underwent multi-environment (including freeze-thaw, acid, etc.) indoor weathering experiments. In this study, the freeze-thaw, acid, and alkaline simulated weathering experiment cycles were each conducted 65 times. After every 5 cycles, 3 samples were preserved from each group for destructive testing, while another 3 fresh blank control samples were stored, totalling 42 rock samples per group. The selected 126 sandstone samples were divided into 3 groups of 42 rock samples each, numbered and prepared for testing. For the freeze-thaw cycle experiment, the 42 sandstone samples underwent different numbers of weathering cycles. The fresh blank rock samples were untreated, while the remaining 39 rock samples simultaneously underwent the freeze-thaw cycle experiment. The specific steps of the freeze-thaw cycle experiment is shown in Figure 1. After every 5 cycles, the rock samples were dried and underwent non-destructive testing, with data recorded. After non-destructive testing, 3 sandstone samples corresponding to the cycle number were preserved for non-destructive testing, while the remaining rock samples

underwent vacuum saturation water absorption treatment in preparation for the next freeze-thaw cycle, until the 65th freeze-thaw cycle was completed.

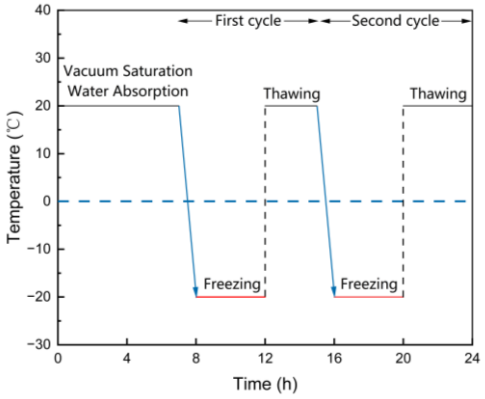

Figure 1. Experimental procedure of Freeze-thaw cycle.

In the acid and alkali solution cycle experiments (Figure 2), each group of 42 sandstone samples underwent varying numbers of weathering cycles. The fresh blank rock samples remained untreated, while the remaining 39 rock samples in each group were subjected to either acid or alkali cycles, respectively. The specific steps involved in the acid-alkali cycle experiments are illustrated in the diagram. After every 5 cycles, the rock samples were dried and subjected to non-destructive testing, with data recorded accordingly. Following the non-destructive testing, 3 sandstone samples corresponding to each cycle number were preserved for destructive testing, while the remaining rock samples were prepared for immersion in the respective acid or alkali solution for the next cycle, until the completion of the 65th cycle for both acid and alkali environments.

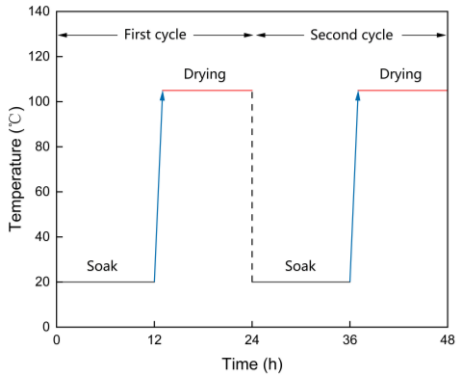

Figure 2. Experimental procedure of dry-wet cycles with acidic and alkaline.

During the experiment process, various non-destructive detection techniques were employed to obtain changes in sandstone samples’ performance, such as mass, ultrasonic wave velocity, and chemical element content.

3.2 XRD&SEM

X-ray diffraction (XRD) and scanning electron microscopy (SEM) are crucial techniques employed to analyze the phase changes in sandstone before and after the experiments. For XRD characterization, a Smartlab X-ray diffractometer was utilized, with a measurement angle range of 10°-90° and an angular accuracy of 0.0001°. SEM characterization was facilitated by a Zeiss GeminiSEM 300 field emission scanning electron microscope, boasting a resolution of 1.0 nm, enabling clear observation of changes in the pore structure even at the nanoscale. The sampling positions for XRD and SEM analyses are illustrated in Figure 3.

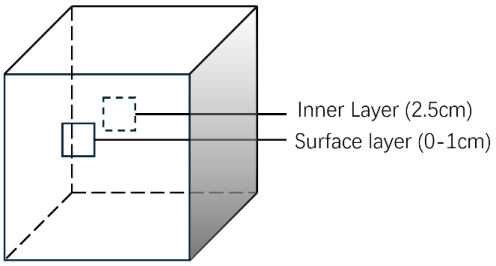

Figure 3. Schematic of XRD and SEM sampling locations.

4. Data and Problem Formulation

4.1 Data Description

After the experiments, a total of 312 data entries were obtained for each deteriorative environment. Every data entry encompassed the iteration number, serving as an indicator of the weathering degree, as well as the variations in nine parameters compared to the initial state prior to the experiments. These parameters included changes in mass and elemental content (comprising Al, Si, Ca, Fe, K), along with the ultrasonic wave velocities measured across three dimensions (x, y, z).

4.2 Feature Construction

In the process of the cyclic experiment, changes in performance parameters such as mass, ultrasonic wave velocity, and chemical element content were measured. The parameters of the samples were recorded before the experiment and after every 5 cycles, and the rate of change for each parameter was calculated to assess the deterioration of the sandstone under different cycles. Taking mass as an example, the formula for the mass change rate is given as:

$$\frac{\Delta M}{\Delta t} = \frac{m_i - m_0}{m_0} \times 100\%, \quad (1)$$

where $\frac{\Delta M}{\Delta t}$ is the mass change rate.
m_i is the mass of the sample after the i^{th} cycle.
m_0 is the initial mass of the sample.

Similarly, the rate of change of ultrasonic wave velocity in three dimensions, V_x, V_y, V_z, can be calculated, as well as the rate of change of each element (Al, Si, Ca, Fe, K). For subsequent input into the model, the iteration count for each sample is used as the label L, and these indicators are encoded as a 1×9 input sequence, represented as X:

$$X_i = [M \quad V_x \quad V_y \quad V_z \quad Al \quad Si \quad Ca \quad Fe \quad K], \quad (2)$$

Where X_i is the feature tensor for the i^{th} sample.

4.3 Problem Formulation

To analyze the contribution of each feature to the weathering degree for subsequent mechanistic analysis, we need an expression to quantify the impact of each feature on weathering. This will allow us to explain the model's prediction results by

attributing the contributions to the various features involved in the prediction.

Assuming the model's predicted degree of weathering for a sample is y_i, and the baseline of the entire model (usually the mean of the target variable for all samples) is y_{base}. We can calculate the deviation of the predicted value for sample i relative to the baseline value by taking the difference, as shown in expression (3).

$$\phi_i = y_i - y_{\text{base}}, \quad (3)$$

This deviation represents the extent to which the predicted value for sample i deviates from the baseline value.

5. Method

5.1 MLP Layer

The Multilayer Perceptron (MLP) is a flexible mathematical modeling technique used to learn the behavior of complex systems by associating input and output data. When coupled with activation layers, MLPs can capture both linear and non-linear relationships between inputs and targets. Consequently, after learning from a set of samples, an MLP can provide solutions for new samples based on the learned patterns. Thus, after training on a portion of experimental data, it can predict the degree of weathering for the remaining data.

An MLP typically comprises an input layer, one or more hidden layers, and an output layer (Figure 4). The number of neurons in the input and output layers corresponds to the dimensions of the input and output data for the problem at hand. However, determining the optimal number of neurons in these layers often requires iterative experimentation. Additionally, the Rectified Linear Unit (ReLU) function is introduced as an activation layer:

$$f(x) = \max(0, x), \quad (4)$$

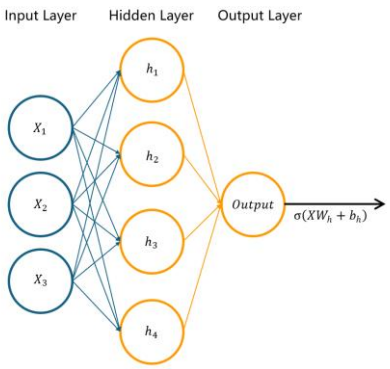

Figure 4. The structure of MLP.

5.2 Multi-attention Layer

The Attention Mechanism is a technique that mimics the human attention process and has achieved significant success in the field of deep learning. Its main idea is to consider that different parameter changes have varying effects on the final degree of weathering. Therefore, we employ the attention mechanism to adaptively capture the influence of each parameter on the weathering degree (Figure 5). This encourages the model to focus more on parameter changes relevant to the task while ignoring less relevant features.

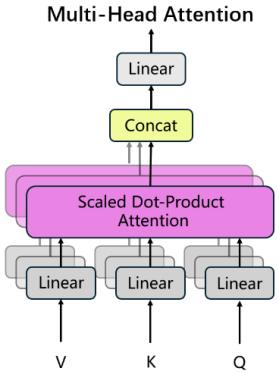

Figure 5. The structure of multi-head attention layer.

For an input feature group X_i with a length of n experimental parameters, where the rate of change of the j^{th} experimental parameter is X_{ij}, we map it to three vectors: query vector Q_i, key vector K_i, and value vector. V_i. Our calculation process involves comparing the distance relationship between the query Q and the key K, then looking up the key K and value V pairs, preferentially inferring the final result. The calculation of these three vectors is obtained through linear mapping of X_i.

$$q = W_q X_i, \quad k = W_k X_i, \quad v = W_v X_i, \quad (5)$$

where W_q, W_k, W_v are mapping matrices for queries, keys, and values, respectively.

Then, we calculate the dot product of the query vector and the key vector, then divide by the square root of the dimension of $\sqrt{d_k}$(where d_k is the dimension of the query or key vector) to obtain attention scores (represented as *Score* here).

$$Score(q, k_i) = \frac{q \cdot k_i}{\sqrt{d_k}}, \quad (6)$$

We normalize the attention scores using the softmax function to obtain attention weights. These weights represent the relative importance of each experimental parameter of each experimental data for the current position output. Here, these weights are denoted as *Weight*.

$$Weight(q, k_i) = \frac{\exp(Score(\mathrm{q}, \mathrm{k_i}))}{\sum_{\mathrm{j}=1}^{\mathrm{n}} \exp(Score(\mathrm{q}, \mathrm{k_j}))}, \quad (7)$$

The attention weights were used to perform a weighted sum on the numerical vectors, obtaining the output of self-attention, denoted as *O*.

$$O(q, \{k_i\}, \{v_i\}) = \sum_{i=1}^{n} Weight(q, k_i) \cdot v_i, \quad (8)$$

By this method, we need to iterate over all feature vectors, and we can convert the above vector calculations into matrix form. We can define multiple sets of Q, K, V, each focusing on different contextual relationships. The calculation process remains the same, except that the matrix for linear transformation changes from a single set of linear mapping matrices to multiple sets of linear mapping matrices. This is the principle of multi-head attention mechanism.

5.3 Linear Interpolation

To increase the generalization of the model by introducing new samples, we employed a linear interpolation method similar to Sample Pairing during the training phase. The interpolation method is shown in Figure 6: for each experimental data entry that will participate in the training, we select another experimental data entry that has not been included in the training

set, and take the average of their respective degrees of weathering (i.e., labels) and feature tensors. Ultimately, as illustrated in Figure 6, we generate a new data entry to replace the original one, which is then fed into the training network for model training.

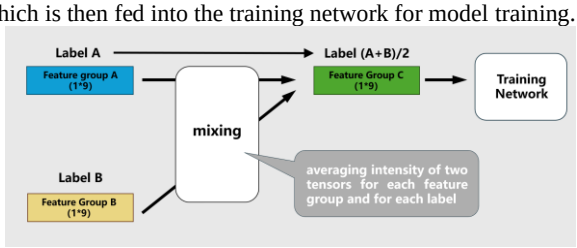

Figure 6. The workflow of linear interpolation.

Specifically, during the training process, our training procedure follows the method proposed by Inoue (Inoue, 2018), as follows:
1) At the beginning of training, we do not enable interpolation training, allowing the loss to quickly converge within the constrained space.
2) During the middle stages of training, we start linear interpolation, and the loss begins to oscillate.
3) After 8 epochs of interpolation, we will turn off linear interpolation for 2 epochs.
4) Once the oscillation becomes stable, we will turn off linear interpolation until the end of training.

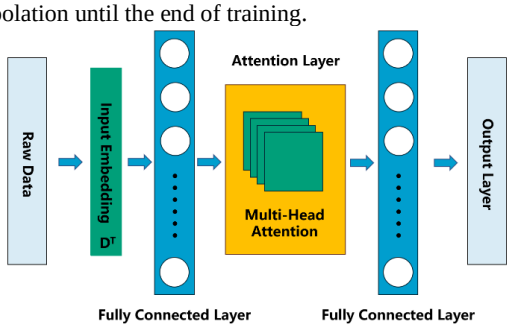

Figure 7. The structure of MLP-ATTENTION Model.

Therefore, the structure of the MLP-Attention-Linear interpolation model is illustrated in Figure 7.

5.4 SHAP

The SHapley Additive exPlanations (SHAP) value is a method employed to interpret predictions generated by machine learning models. It is rooted in the concept of Shapley values originating from game theory, applied in this context to quantify the contribution of each experimental parameter to the output weathering degree. The core principle of SHAP values lies in allocating the contribution of each feature to the various features involved in the prediction, thereby elucidating the model's prediction results. It takes into account all possible combinations of features and calculates the impact of features on the model output for each combination. Assuming the i-th experimental sample is represented by x_i and the j^{th} experimental parameter feature of the i^{th} sample is x_{ij}, then the SHAP value follows the following equation:

$$\phi_i = \sum_{j=1}^{M} f(x_{i,j}), \quad (9)$$

For a given feature, a higher SHAP value indicates a greater contribution of that input experimental parameter feature to the degree of weathering.

6. Result and Discussion

6.1 Model Performerce

To observe the improvements in the model after incorporating the attention mechanism and linear interpolation, we first take the freeze-thaw data as an example and perform regression with different detection parameters as independent variables and the number of cycles as the dependent variable. In this setting, the learning rate is fixed at 0.01, the number of iterations is fixed at 300, 20% of the data is used as the validation set, and the mean square error (MSE) is used as the loss metric. Compared to a model consisting of only two MLP layers, the introduction of the attention mechanism layer reduces the MSE loss on the test set from 66.47 to 7.14, although the training time increases. After adding linear interpolation to the training process, the training duration is further prolonged (because linear interpolation consumes considerable computational resources), but the MSE loss on the test set further decreases to 2.58.

Model	Learning Rate	Number of iterations	Training time(S)	Test MSE
MLP	0.01	300	2.80	66.47
MLP-Attention	0.01	300	90.67	7.14
MLP-Attention-Linear interpolation	0.01	300	1,032.51	2.58

Table 1. Deep-learning parameters and classification accuracy.

From the training loss curve in Figure 8, it can be observed that there are expected oscillations in the middle stage (epochs 50-220). According to the magnified part of the graph, it can be inferred that in the final stage after turning off linear interpolation, the MLP Attention Linear Interpolation model converges more quickly to the low loss range, clearly achieving the best effect. On the test set, the MLP Attention Linear Interpolation model achieves the best results, and the losses are compared, indicating that the generalization advantage provided by linear interpolation is more obvious. Therefore, for data from different experimental environments, this paper trains the MLP Attention Linear Interpolation model and then uses SHAP for factor analysis.

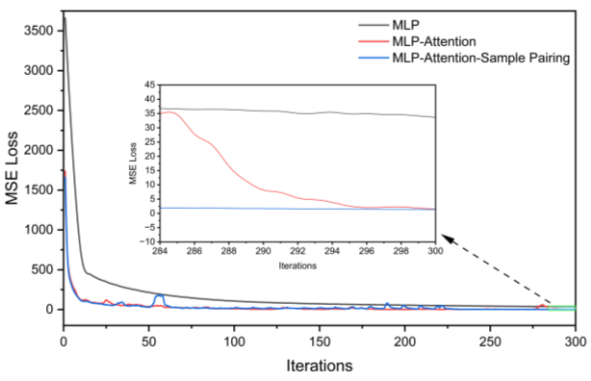

Figure 8. The loss curves of the three models.

6.2 Factor Analysis with SHAP

Through SHAP analysis, the main detection techniques strongly associated with the number of weathering cycles were determined.

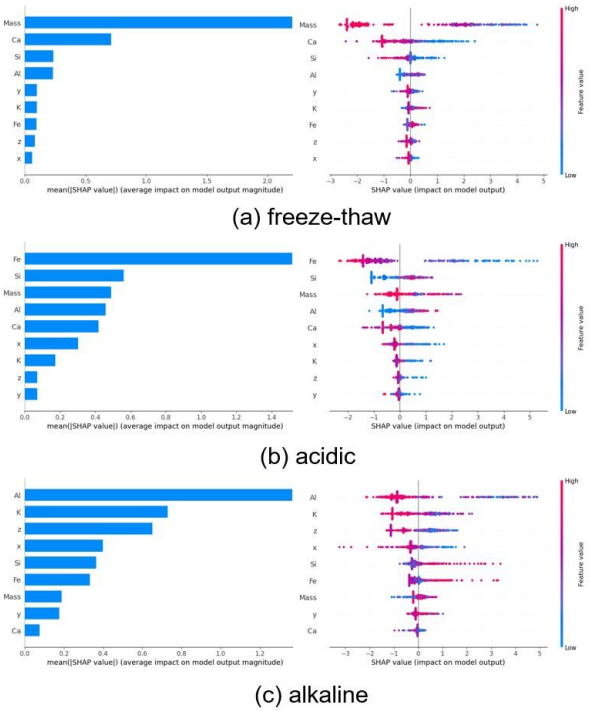

Figure 9. Scatter plots and bar graphs of SHAP factor analysis in multiple environments including: (a) freeze-thaw, (b) acidic, (c) alkaline.

As Figure 9 suggests, under freeze-thaw conditions, the main indicators that change are the total mass and the content of Ca. The scatter plot shows that as the number of cycles increases, both the total mass and the content of Ca gradually decrease. Calcium is a major element in the composition of sandstone feldspar, calcite, dolomite, and other metallic minerals. The decrease in Ca content indicates, to a certain extent, a reduction in the content of these mineral components. A decrease in the content of cementing materials leads to a decline in the cementation ability of sandstone, resulting in the shedding of mineral particles. Under freeze-thaw conditions, the influence of chemical composition is relatively small; therefore, the proportion of mass change is relatively large.

Under acidic conditions, the main changes are in the content of iron and silicon elements. The scatter plot shows that as the number of cycles increases, the mass of Fe decreases, while the content of Si increases. The decrease in iron content is due to the dissolution reactions of feldspar, calcite, dolomite, metallic iron, and their oxides in acidic solutions. After feldspar, cementing material calcite, and dolomite are eroded by acidic solutions, they undergo chemical reactions to form gypsum (CaSO4) and other sulfate substances. The solution will migrate into the sandstone's interior through its pores and channels. The inner cementing material will also undergo the same chemical reactions to generate sulfates, which will dissolve in water or form salt crystals. Therefore, after cycling, the content of elements such as Fe decreases in the sandstone.

Under alkaline conditions, the most significant changes observed are the variations in Al and K elemental content. The scatter plot shows that with the accumulation of cycle numbers, the content of Al and K elements gradually decreases. The sandstone mainly undergoes dissolution reactions of quartz and feldspar in alkaline solutions, and form salt substances such as sodium silicate, calcium silicate, and potassium silicate. Therefore, after cycling, the content of elements such as Al and K decreases in the sandstone.

6.3 Mineral Composition and Microstructure Analysis

According to the XRD test results, the main mineral components of fresh sandstone include quartz (SiO_2), potassium feldspar ($KAlSi_3O_8$), calcite ($CaCO_3$), and kaolinite ($Al_2Si_2O_5(OH)_2$). However, the mineral composition of sandstone varies under different environmental conditions. In the freeze-thaw cycle experiment, characteristic peaks of quartz, potassium feldspar, calcite, and kaolinite were observed at all stages. After the cycles, the intensity of the calcite peak slightly decreased, the potassium feldspar peak intensity reduced, and the kaolinite peak intensity increased, indicating a decrease in potassium feldspar content and an increase in kaolinite content.

In the acidic cycle experiment, characteristic peaks of quartz, potassium feldspar, and kaolinite were observed at all stages. The characteristic peak of calcite gradually weakened and became extremely low after 60 cycles. New characteristic peaks of salt substances $CaSO_4$ and $MgSO_4$ were detected, indicating that the mineral components underwent chemical dissolution reactions.

In the alkaline cycle experiment, characteristic peaks of quartz, potassium feldspar, and kaolinite were observed at all stages. After 60 cycles, the characteristic peaks of potassium feldspar and calcite significantly weakened, and new peaks of sodium silicate appeared. This suggests that the content of potassium feldspar and calcite decreased, and the sandstone structure was damaged.

Additionally, SEM was used to observe and analyze the microstructure characteristics of the surface (0-0.5 cm) and inner layer (2-2.5 cm) of the sandstone. The magnification used was 1000 and 3000 times, respectively. The top-left image is a 1000x magnification morphology image of the surface, the top-right image is a 3000x magnification morphology image of the surface, the bottom-left image is a 1000x magnification morphology image of the inner layer, and the bottom-right image is a 3000x magnification morphology image of the inner layer.

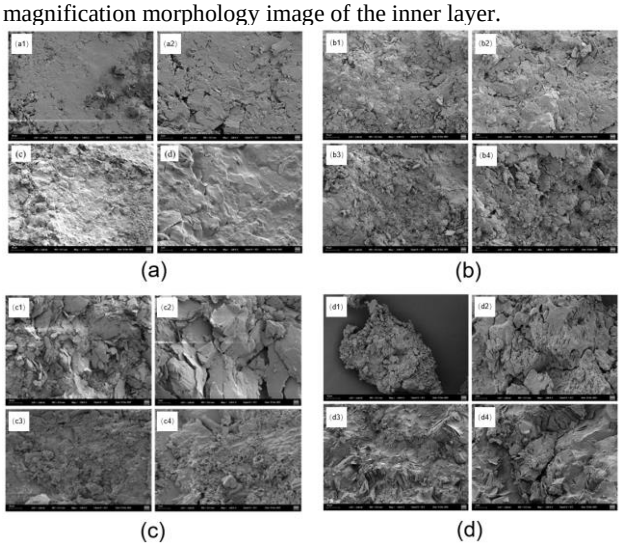

Figure 10. SEM microstructure images of sandstone under weathering in multiple environments, including: (a) fresh, (b) freeze-thaw, (c) acidic, (d) alkaline.

The SEM images in Figure 10 clearly demonstrate that the microstructure of both the surface and inner layers of fresh sandstone is compact, with well-defined particle outlines, strong cementation, and a smooth surface.

There are few signs of weathering, with only a small number of tiny pores present on the surface, while the inner layer is nearly pore-free, suggesting a high degree of density. Following the alkaline cycling experiment, both the surface and inner layers of the sandstone exhibited pronounced weathering characteristics. The sandstone's surface structure became loose, with numerous irregularly distributed mineral particles of varying sizes and a significant amount of fine debris adhering to it. At higher magnifications, multiple micro-cracks and pores were visible on the sandstone surface. The primary cause of this weathering is the dissolution of quartz and feldspar within the sandstone when exposed to alkaline conditions, resulting in the formation of dissolution holes on the surface. This process erodes the structure, weakens the cementation between particles, and leads to the generation and precipitation of new salts, which accumulate as fine mineral particles on the surface. In contrast, the inner layer of the sandstone remained free of debris particles and maintained a relatively intact structure. The surface displayed minor undulations, with some degree of cementation between mineral particles. Under magnification, micro-cracks and a small number of dissolution pores were still observed. However, when compared to fresh sandstone, the inner layer structure also exhibited some damage, although to a lesser extent than the surface.

7. Conclusion

Detecting and assessing the condition of stone cultural heritage is of utmost importance. In this study, a method utilizing deep learning techniques to analyze the adaptability of deterioration detection technologies for stone cultural relics was proposed. Firstly, weathered sandstone samples were prepared under four conditions (freeze-thaw, acidic, and alkaline) through laboratory-simulated weathering experiments. Detection parameters of the sandstone under different weathering environments were obtained using various non-destructive detection techniques, such as ultrasonic wave velocity detection and XRF detection. Next, an MLP-Attention-Linear interpolation model was developed to analyse the relationship between the above NDT parameters and the degree of weathering. The SHAP technique was then used to analyse the contribution of each detection parameter to the weathering degree under different environmental conditions, i.e. the correlation between the detection parameters and the degree of weathering. The results show that the applicability of various detection techniques in assessing sandstone deterioration under different environmental conditions varies widely. Combined with further chemical composition and microstructural analyses, it is evident that the correlation of these detection parameters is closely related to the changes in microstructure and chemical composition of the sandstone during the deterioration process. These findings emphasise the importance of selecting the most appropriate and effective assay parameters and techniques for assessing stone deterioration in response to the specific environmental challenges faced by stony cultural heritage.

Acknowledgments

This research was supported by Research Project of Shanxi Cultural Relics Bureau (No. 2024KT19), Scientific and Technological Research Project on Cultural Relics (No. 2023ZCK014), Science and Technology Major Special Program Project of Shanxi Province (No. 202201150501024) and Project of Key Laboratory of Silicate Cultural Relics Conservation (Shanghai University), Ministry of Education (No. SCRC2024ZZ02ZD).

References

Ceryan S., Zorlu K., Gokceoglu C., Temel A., 2008: The use of cation packing index for characterizing the weathering degree of granitic rocks. *Eng Geol*, 98(1-2), 60-74. doi.org/10.1016/j.enggeo.2008.01.007.

El-Gohary M. A., 2013: Evaluation of treated and un-treated Nubia Sandstone using ultrasonic as a non-destructive technique. *J. Archaeol Sci*, 40(4), 2190-5. doi.org/10.1016/j.jas.2012.12.023.

Fioretti G., Andriani G. F., 2018: Ultrasonic wave velocity measurements for detecting decay in carbonate rocks. *Q. J. Eng. Geol. Hydrogeo.*, 2(51), 179-86. doi.org/10.1144/qjegh2016-110.

Friolo K. H., Stuart B., Ray A., 2003: Characterisation of weathering of Sydney sandstones in heritage buildings. *J. Cult Herit*, 4(3), 211-20. doi.org/10.1016/S1296-2074(03)00047-5.

Hachinohe S., Hiraki N., Suzuki T., Chigira M., 2000: Rates of weathering and temporal changes in strength of bedrock of marine terraces in Boso Peninsula, Japan. *Eng Geol*, 55(1-2), 29-43. doi.org/10.1016/S0013-7952(99)00104-0.

Huang J., Zheng Y., Li H., 2022: Study of internal moisture condensation for the conservation of stone cultural heritage. *J. Cult Herit*, 56(1-9. doi.org/10.1016/j.culher.2022.05.003.

Jayawardena U. D. S., Izawa E., 1994: A new chemical index of weathering for metamorphic silicate rocks in tropical regions: A study from Sri Lanka. *Eng Geol*, 36(3–4), 303-10. doi.org/10.1016/0013-7952(94)90011-6.

Sousa L. M. O., Suárez Del Río L. M., Calleja L., Ruiz De Argandoña V. G., Rey A. R., 2005: Influence of microfractures and porosity on the physico-mechanical properties and weathering of ornamental granites. *Eng Geol*, 77(1-2), 153-68. doi.org/10.1016/j.enggeo.2004.10.001.

Wang X., Cheng Y., Zhang R., Zhang Y., Huang J., Yan H., 2024: Non-Destructive Assessment of Stone Heritage Weathering Types Based on Machine Learning Method Using Hyperspectral Data. *Int. Arch. Photogramm. Remote Sens. Spatial Inf. Sci.*, XLVIII-1-2024, 713-719. doi.org/10.5194/isprs-archives-XLVIII-1-2024-713-2024.

Yang H., Ni J., Chen C., Chen Y., 2023: Weathering assessment approach for building sandstone using hyperspectral imaging technique. *Herit. Sci.*, 11(1). doi.org/10.1186/s40494-023-00914-7.

Zhang Y., Cao C., Du H., Huang J., Guo X., Luo Q., Ren J., 2023: Investigation into the Gaseous SO2 Attack on Sandstone in the Yungang Grottoes. *Minerals (Basel)*, 13(1), 123. doi.org/10.3390/min13010123.

Zhang Y., Zhang Y., Huang J., 2022: Experimental study on capillary water absorption of sandstones from different grotto heritage sites in China. *Herit. Sci.*, 10(1). doi.org/10.1186/s40494-022-00656-y.